

Secure optical interconnects using orbital angular momentum beams multiplexing/multicasting

Yifan Zhao,^{a,b,c} Jun Liu,^{a,b,c} Shuhui Li,^{a,b,c} Andong Wang,^{a,b,c} Long Zhu,^{a,b,c} Yan Luo,^{a,b,c} Shi Chen,^{a,b,c} Nan Zhou,^{a,b,c} Shuang Zheng,^{a,b,c} Jing Du,^{a,b,c,*} and Jian Wang^{a,b,c,*}

^aHuazhong University of Science and Technology, Wuhan National Laboratory for Optoelectronics and School of Optical and Electronic Information, Wuhan, China

^bOptics Valley Laboratory, Wuhan, China

^cShenzhen Institute of Huazhong University of Science and Technology, Shenzhen, China

Abstract. Orbital angular momentum (OAM), described by an azimuthal phase term $\exp(jl\theta)$, has unbound orthogonal states with different topological charges l . Therefore, with the explosive growth of global communication capacity, especially for short-distance optical interconnects, light-carrying OAM has proved its great potential to improve transmission capacity and spectral efficiency in the space-division multiplexing system due to its orthogonality, security, and compatibility with other techniques. Meanwhile, 100-m free-space optical interconnects become an alternative solution for the “last mile” problem and provide interbuilding communication. We experimentally demonstrate a 260-m secure optical interconnect using OAM multiplexing and 16-ary quadrature amplitude modulation (16-QAM) signals. We study the beam wandering, power fluctuation, channel cross talk, bit-error-rate performance, and link security. Additionally, we also investigate the link performance for 1-to-9 multicasting at the range of 260 m. Considering that the power distribution may be affected by atmospheric turbulence, we introduce an offline feedback process to make it flexibly controllable.

Keywords: orbital angular momentum; free-space optical interconnects; security; space-division multiplexing; multicasting.

Received Jul. 14, 2023; revised manuscript received Oct. 25, 2023; accepted for publication Nov. 29, 2023; published online Dec. 15, 2023.

© The Authors. Published by SPIE and CLP under a Creative Commons Attribution 4.0 International License. Distribution or reproduction of this work in whole or in part requires full attribution of the original publication, including its DOI.

[DOI: [10.1117/1.APN.3.1.016004](https://doi.org/10.1117/1.APN.3.1.016004)]

1 Introduction

The unabated exponential growth of global communication traffic has fueled ever-increasing research efforts for sustainable expansion of transmission capacity.¹ To meet the need for transmission capacity, multiplexing in polarization and wavelength, known as polarization-division multiplexing and wavelength-division multiplexing,^{2,3} and different multilevel modulation, such as m-ary phase-shift keying and m-ary quadrature amplitude modulation⁴ have been used to improve transmission capacity and efficiency. However, with the flourishing of optical interconnects, those mentioned techniques fail to meet the

increasing system capacity demand. As another alternative approach for optical communication, space-division multiplexing (SDM) has attracted incremental interest for its potential to dramatically increase system capacity by a factor equal to the number of transmitted orthogonal modes.^{5,6}

One potential orthogonal modal basis set is the orbital angular momentum (OAM) mode, sometimes called twisted beam, which is featured by a helical phase front of $\exp(i\ell\theta)$ that carries an OAM corresponding to $\ell\hbar$ per photon (where ℓ is the topological charge, θ is the azimuthal angle, and \hbar is the reduced Planck's constant).⁷ After first demonstrated in the labs by Allen et al.,⁷ OAM has given rise to many developments in optical tweezers, optical trapping, optical manipulation, optical vortex knots, astronomy, imaging, and quantum information transmission and processing.^{8–22} Additionally, it has some inherent properties of

*Address all correspondence to Jing Du, jing_du@hust.edu.cn; Jian Wang, jwang@hust.edu.cn

OAM modes, such as orthogonality,⁷ security,⁵ and compatibility with other multiplexing techniques,⁶ which provide its great potential in optical communication both in optical fiber²³ and free space.⁶ Meanwhile, system capacity and spectral efficiency have reached laudable 1.036-Pbit/s²⁴ and 435-bit/s/Hz²⁵ in free space employing both OAM multiplexing and other techniques. However, those mentioned works were demonstrated in labs at the range of a few meters, which ignores the influence of OAM modes resulting from the real atmospheric turbulence.

Over the past decades, free-space optical (FSO) communication in practical applications remained mainly confined to military applications,^{26,27} intersatellite links,²⁸ and deep-space links.^{29,30} However, in recent years, with the development of techniques and the increasing demand for transmission capacity in optical interconnects, a growing number of research institutes and companies offer solutions and products in visible, infrared, and ultraviolet bands,^{6,31,32} the market has begun to show promise. Considering multiple increases in system capacity and spectral efficiency by employing OAM multiplexing, it is meaningful to exploit this dimension in FSO interconnects. Unfortunately, there are still some challenges; for example, inhomogeneity in the pressure and temperature or the dust in the atmosphere results in variations of the refractive index along the transmission path, which can degrade the performance of an optical interconnects link, especially for OAM multiplexing communication link. Some reports evaluated the performance of long-distance free-space OAM transmission links and demonstrated the information transfer.^{33,34} Very recently, a laudable experiment reported that multiplexing of four collocated OAM beams achieved a 120-m 400-Gbit/s FSO communications link.³⁵ To the best of our knowledge, security FSO interconnects over hundreds of meters using OAM multiplexing and multicasting have not yet been studied.

In this paper, we experimentally demonstrate a 260-m secure FSO interconnect using spatial multiplexing of two OAM beams, where each channel is modulated with a 10-Gbaud (40-Gbit/s) 16-ary quadrature amplitude modulation (16-QAM) data signal.³⁶ We study the OAM link performance after 260-m propagation, including beam wandering, received power fluctuation, channel cross talk, bit error rate (BER), and link security. The obtained results show that the average mode cross talk is less than -20 dB when demultiplexing by a full pattern and

it degrades to ~ -10 dB when demultiplexing by an angular 1/4-block pattern, which indicates the 260-m security OAM transmission link. Furthermore, 260-m power-controllable 1-to-9 multicasting interconnects are also demonstrated utilizing an offline feedback process to redistribute power among nine channels according to the demand. The BER performance shows its only ~ 2 dB optical signal-to-noise ratio (OSNR) penalty compared to the back-to-back (B2B) curve at enhanced forward error correction (EFEC) threshold of 2×10^{-3} .

2 Results

2.1 Concept, Principle, and Experimental Setup

Hundreds of meters are an appropriate range for interbuilding interconnects, which have been booming recently as an alternative solution for the “last mile” problem.^{37–41} Figure 1 (upper row) illustrates the concept and principle of a 260-m secure optical interconnect link employing two distinguished OAM channels multiplexing between two buildings. Moreover, this link can also be used for 1-to- N OAM multicasting. Because all of space is full of atmospheric turbulence, the property of OAM modes will be affected (by, for example, beam wander and phase distortion), resulting in degradation of signal performance. Additionally, there is another distinct advantage: that OAM can lead to improved security to an optical interconnects link. The eavesdropper cannot measure accurate OAM information while wiretapping an angular of $< 2\pi$. As shown in the upper row in Fig. 1, the eavesdropper wiretaps a part of OAM beams and he obtains a terrible signal performance that provides the link security. The layout of our experiment is also illustrated in Fig. 1 (lower row). The OAM multiplexing/multicasting FSO interconnect link is exposed to the atmospheric conditions between the corridors from WNLO-E building to WNLO-H building (WNLO, Wuhan National Laboratory for Optoelectronics). The transmitter and the receiver are located at the front of the gate of the WNLO-E building and the reflection mirror (M) is located at the end of the corridors. The single-way distance is 130 m; thus, the total distance of double-pass transmission is 260 m after reflection.

The experimental setup is shown in Fig. 2. A narrow line-width laser at 1550 nm is sent to an IQ modulator to produce

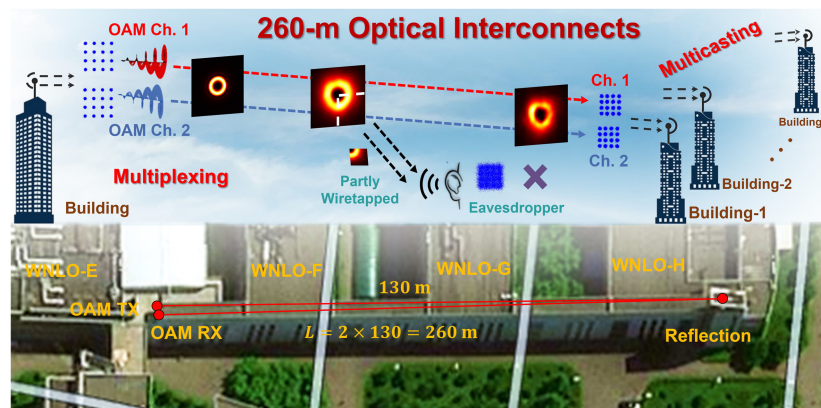


Fig. 1 Concept and principle. Upper row: concept of an interbuilding optical interconnects employing OAM multiplexing/multicasting and shows its security. Lower row: layout of a 260-m security OAM multiplexing/multicasting FSO interconnect link between WNLO-E building and WNLO-H building. WNLO, Wuhan National Laboratory for Optoelectronics.

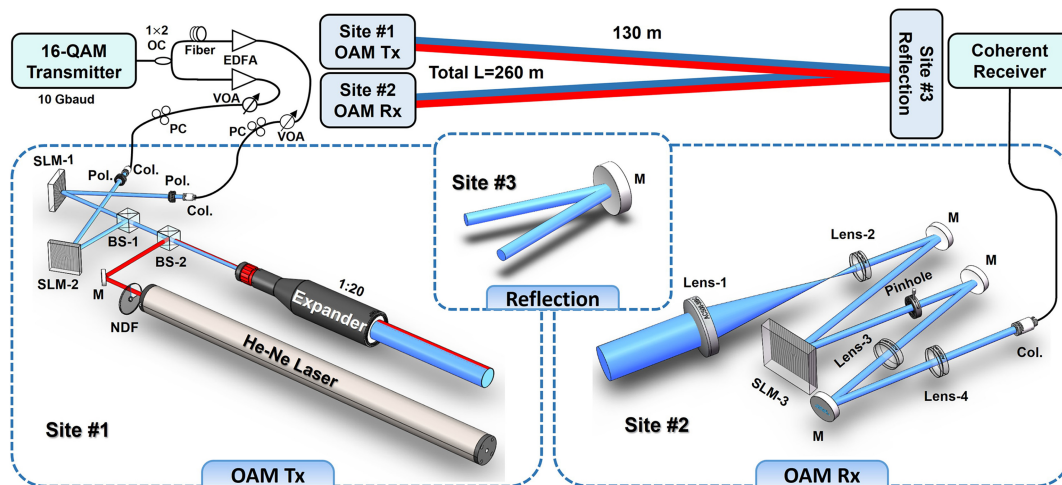


Fig. 2 Experimental setup for 260-m security OAM multiplexing/multicasting link. SLM-1, spatial light modulation; Pol., polarizer; Col., collimator; BS, beam splitter; PC, polarization controller; VOA, variable optical attenuator; OC, optical coupler; EDFA, erbium-doped fiber amplifier; M, mirror; NDF, neutral density filter; Tx, transmitter; Rx, receiver. The practical picture for site #1, site #2, and site #3 are presented in Fig. S2 in the [Supplementary Material](#).

a 10-Gbaud (40-Gbit/s) 16-QAM signal (refer to Fig. S1 in the [Supplementary Material](#)). The 16-QAM signal is split into two copies for two OAM channels. In one copy, the signal is delayed with a 2-km single-mode fiber (SMF) to decorrelate the data sequence, and thus the two channels are decorrelated. Before connecting to collimators, the two channels are sent to an erbium-doped fiber amplifier, variable optical attenuator, and polarization controller for proper power and polarization control. The two spatial light modulators (SLMs) in two paths modulate the light beams to OAM state $l = +3$. After a combination using a beam splitter (BS-1) with the OAM state reversed in the reflective path (mirror image effect), two OAM beams with opposite states are multiplexed together ($l = \pm 3$). Meanwhile, a He-Ne laser at 632.8 nm produces a clear Gaussian beam (size, 0.8 mm), which is combined with the two OAM channels using another beam splitter (BS-2). This red Gaussian beam is mainly used for easy system alignment. The two OAM channels and the red beam pass through a 1:20 expander with the beam size magnified to ~ 4 cm. Note that we can produce a converged beam by sliding the lens adjustment and adjusting the beam waist position at the reflection site in the end of corridor (see [Supplementary Material](#) for more details). As a result, we can receive a ~ 4 cm beam in the OAM RX.

The received OAM beam size is reduced by two lenses ($f = 300$ and 40 mm), but still converged. At the proper position, the OAM channel can be demodulated by loading an inverse fork hologram pattern on SLM-3. After a telescope system ($f = 50$ and 400 mm), the converged demodulated beam is magnified and collimated and then coupled into an SMF for coherent detection assisted by offline digital signal processing (see Fig. S1 in the [Supplementary Material](#)).

2.2 Intensity Profiles and Beam Fluctuation after 260-m Transmission

Figure 3 shows the intensity profiles of generated OAM beams with a topological charge of $l = +3$ and $l = -3$ (a1), (a2), their

superposition (a3), and interferograms with Gaussian beam (a4), (a5) at the transmitter side. Correspondingly, the intensity profiles of received OAM beams after 260-m propagation are also displayed in Figs. 3(b1)–3(b5). In fact, we recorded the intensity profiles and interferograms covering the topological charge from $l = -6$ to $l = +6$, excluding the Gaussian beam (refer to Fig. S3 in the [Supplementary Material](#)). Meanwhile, Figs. 3(c1)–3(c4) illustrate the demodulated beams for different patterns loaded onto SLM-3 when transmitting $l = -3$. It is found that only when the demodulated pattern is inverse to the transmit OAM state can the OAM beam be converted into a Gaussian-like beam with a bright spot at the beam center (c4). Such a Gaussian-like beam can be coupled into an SMF more efficiently than other demodulated beams.

Owing to the atmospheric turbulence, it is valuable to investigate the fluctuation of demodulated position and received power. Figures 4(a1) and 4(a2) depict the center displacement of the received demodulation beam. It is observed that the maximum displacement is around ~ 0.45 mm for $l = +3$ and ~ 0.5 mm for $l = -3$ (see [Supplementary Material](#) for more details). Figures 4(b1) and 4(b2) present the space light power fluctuation after the beam reduction (the inverse telescope consists of Lens-1 and Lens-2 at the OAM receiver site), and the power is stable, with a slight difference for two channels due to the atmospheric loss. The fluctuations of the received power of the signal channel and cross talk channel after SMF are shown in Figs. 4(c1), (c2) and 4(d1), (d2). The received power fluctuations up to ~ 8 dB for signal channel demultiplexed by $l = +3$, ~ 10 dB for the cross talk channel demultiplexed by $l = +3$, ~ 4 dB for signal channel demultiplexed by $l = -3$, and ~ 6 dB for the cross talk channel demultiplexed by $l = -3$ are observed within a 50% probability distribution range (see [Supplementary Material](#) for details). The cross talk between the two channels is ~ -20 dB ($l = +3$) and ~ -24 dB ($l = -3$), which provides for the possibility of employing OAM multiplexing and other advanced modulated techniques. All the received data are recorded in 200 s at the interval of 1 s.

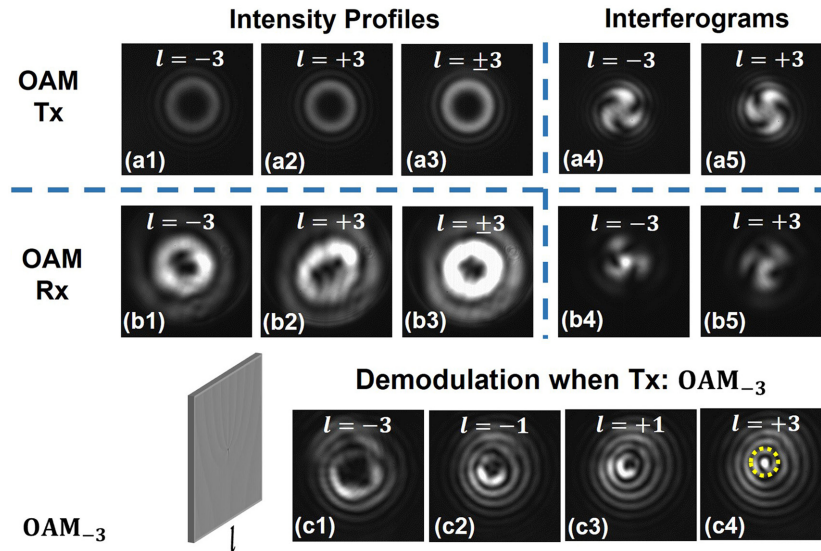


Fig. 3 Generated OAM beams for (a1) $l = -3$; (a2) $l = +3$; (a3) superposition of $l = \pm 3$ and interferograms for (a4) $l = -3$; and (a5) $l = +3$ at Tx. Received OAM beams for (b1) $l = -3$; (b2) $l = +3$; (b3) superposition of $l = \pm 3$ and interferograms for (b4) $l = -3$; and (b5) $l = +3$ at Rx. (c1)–(c4) Demodulated beams for different loading patterns ($l = -3, l = -1, l = +1$, and $l = +3$) when transmitting $l = -3$. Tx, transmitter and Rx, receiver.

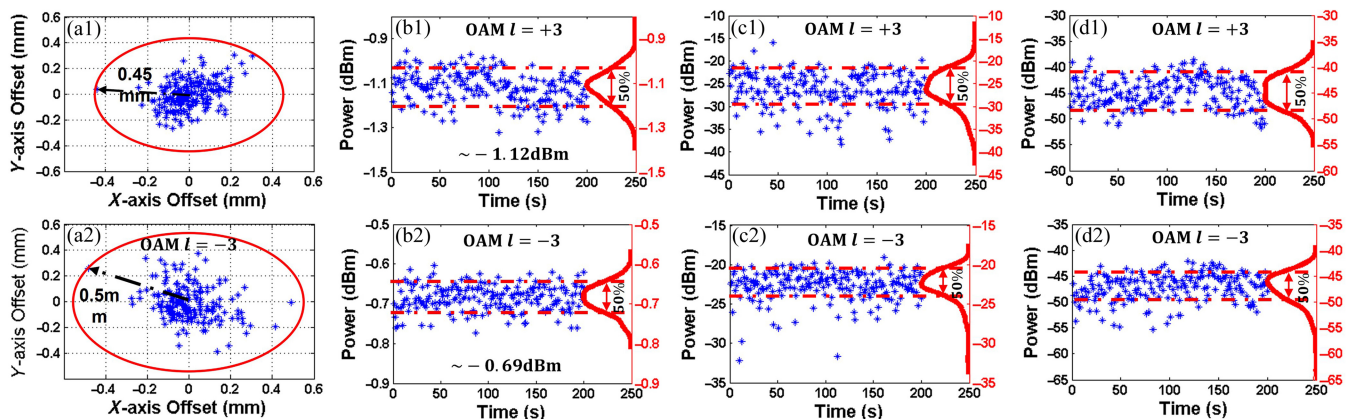


Fig. 4 Statistic results of fluctuations after 260-m OAM multiplexing transmission (recorded in 200 s at the interval of 1 s). (a1), (a2) Center displacement of the received demodulation beam ($l = +3, l = -3$); (b1), (b2) space light-power fluctuation after the beam reduction ($l = +3$ and $l = -3$); (c1), (c2) received power of signal channel after SMF; and (d1), (d2) received power of cross talk channel after SMF.

2.3 BER Performance and Security for Multiplexing Interconnects Link

Furthermore, we demonstrate a 260-m optical interconnect link using 16-QAM carrying OAM multiplexing and also evaluate its BER performance and security (see the first section of the [Supplementary Material](#) for more details about BER measurement). As shown in Fig. 5(a1), we demodulate the received multiplexed OAM beam with a full pattern ($l = +3$ and $l = -3$) on SLM-3. For the BER performance, there is about a 2.5 dB penalty between the B2B curve and the two multiplexing curves at an EFEC threshold of 2×10^{-3} . The constellation diagram is also inserted in Fig. 5(a1), representing the system performance. Figures 5(a2) and 5(a3) illustrate the BER fluctuation with

$l = +3$ and $l = -3$ on SLM-3, respectively, at the OSNR of ~ 18 dB within 25 min at an interval of 1 min. We believe that atmospheric turbulence and building sway are two major reasons leading to this phenomenon. Figures 5(a2) and 5(a3) display the results of BER variations over time when the system operates near the EFEC threshold. It can be observed that at certain moments, the BER exceeds the EFEC threshold. This is attributed to the fact that beam wandering can easily cause the receiver's OSNR to drop below 18 dB, resulting in a BER higher than the EFEC threshold and a degradation in communication quality. However, in practical applications of communication systems, it is typically avoided to operate the communication link near the FEC threshold. Instead, the common practice is to increase the optical power at the transmitter to elevate the receiver's

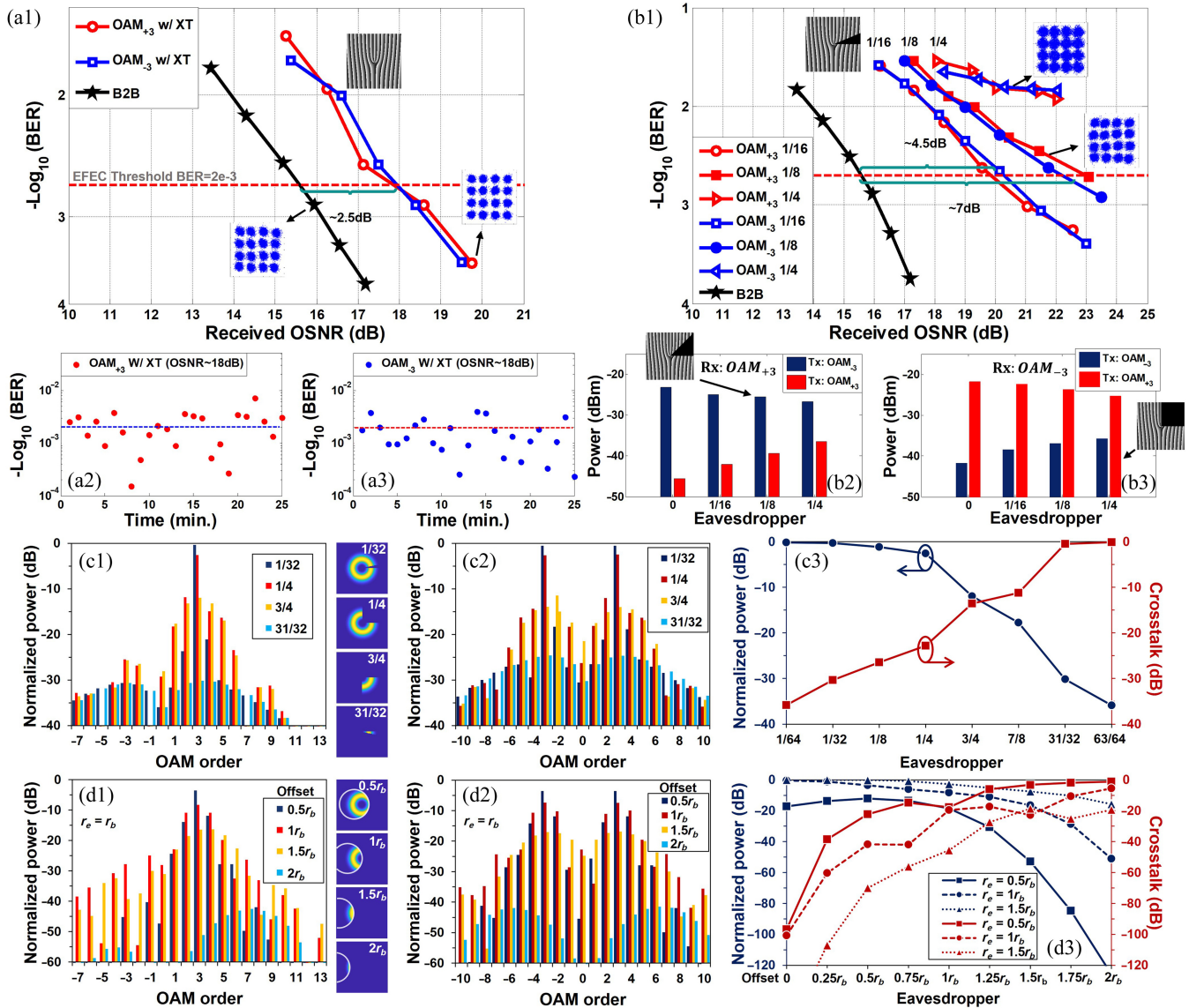


Fig. 5 BER performance for multiplexing. (a1) Measured BER performance for 260-m 10-Gbaud 16-QAM OAM multiplexing FSO interconnect link. (a2), (a3) BER fluctuation with $l = +3$ and $l = -3$ on SLM-3, respectively, at the OSNR of ~ 18 dB. (b1) Measured BER performance for 260-m security OAM multiplexing FSO interconnect link. (b2), (b3) Average received power distribution according to various angular block parts. (c1) Simulated OAM order spectra of OAM beams with $l = +3$ wiretapped by the eavesdropper with angular block. Insets are intensity profiles wiretapped by the eavesdropper. (c2) Simulated OAM order spectra of multiplexed OAM beams with $l = +3$ and $l = -3$ wiretapped by the eavesdropper with angular block. (c3) Simulated normalized power of OAM beam with $l = +3$ and cross talk between OAM beam with $l = +3$ and $l = -3$ wiretapped by the eavesdropper with angular block. (d1) Simulated OAM order spectra of OAM beams with $l = +3$ wiretapped by the eavesdropper in a general scenario. Insets are intensity profiles wiretapped by the eavesdropper. r_e , eavesdropper's aperture radius and r_b , OAM beam radius of $l = +3$ transmitted over 260 m. (d2) Simulated OAM order spectra of multiplexed OAM beams with $l = +3$ and $l = -3$ wiretapped by the eavesdropper in a general scenario. (d3) Simulated normalized power of OAM beam with $l = +3$ and cross talk between OAM beam with $l = +3$ and $l = -3$ wiretapped by the eavesdropper in a general scenario.

OSNR, provide a certain level of redundancy, and stay well clear of the FEC threshold. In the optical communication system we have proposed, as long as the receiver's OSNR exceeds 18 dB, the BER remains below the EFEC threshold. Consequently, in practical applications, error occurrences are minimized.

Moreover, we prove the link security in our 260-m OAM multiplexing optical interconnects. For eavesdroppers, there are only two ways to obtain the transmitted information. The first method is to attempt to recover information from the light scattered by the atmosphere. However, OAM beams suffer severe

phase distortion when scattered by the atmosphere, making demodulating OAM modes nearly impossible. The second method is for eavesdroppers to wiretap partial optical fields along the path of the optical beam, which is the main focus of this paper. This paper primarily discusses the security characteristics of a communication system in an extreme scenario, where the eavesdropper has already determined the topological charge of the OAM mode and the wiretapped optical field exhibits ideal angular distribution characteristics. As shown in Fig. 5(b1), we, respectively, load the 1/16-block, 1/8-block, and 1/4-block pattern onto SLM-3 and present their BER performance demultiplexed by $l = +3$ and $l = -3$. The patterns used here serve the dual purpose of enabling the eavesdropper to wiretap a portion of the optical field and to demodulate the OAM modes for the sake of simplifying the experimental setup. The portion of the patterns with the fork holograms corresponds to what the eavesdropper captures. When the eavesdropper wiretaps a majority of the OAM beams with 1/16-block, the BER curves can be still below the EFEC limit of 2×10^{-3} but with significantly increased OSNR penalty (~ 4.5 dB) compared to the case with a full pattern. Such a phenomenon can be ascribed to the increased OAM channel cross talk when blocking a part of OAM beams, which enhances the security of the OAM multiplexing transmission link. As the blocked part of OAM beams increases, the BER curves degrade rapidly. The OSNR penalty increases to ~ 7 dB when loading a 1/8-block demodulated pattern. When 1/4 part of OAM beams is blocked (1/4-block pattern), the BER performance of the optical interconnect link cannot be below the EFEC limit, i.e., the eavesdropper loses much correct data information. The insert constellation diagram can also explain the degraded tendency. As a consequence, the eavesdropper wiretapping a part of OAM beams fails to get correct data information. The more OAM beams are blocked, the more errors are received by the eavesdropper. Only complete reception of OAM beams corresponds to the best BER performance. From another perspective, the obtained results shown in Figs. 5(b2) and 5(b3) also indicate a successful demonstration of 260-m security FSO interconnect link using 16-QAM carrying OAM multiplexing. As the blocked part increase from 0 to 1/4-block for both demodulated patterns ($l = +3$ and $l = -3$), the received power decreases for the signal channel and increases for the cross talk channel so that the interchannel cross talk increases rapidly (from less than -20 dB to more than -10 dB). The larger the interchannel cross talk is, the more terrible BER performance shows.

To further analyze the mode distribution characteristics of the optical beams wiretapped by eavesdroppers, we simulated the OAM order spectra of the multiplexed OAM beams after a 260-m free-space transmission with different block patterns, as shown in Figs. 5(c1) and 5(c2). Figures 5(c1) and 5(c2), respectively, depict the OAM order spectra obtained by eavesdroppers for an individual OAM beam ($l = +3$) and two OAM multiplexed beams ($l = +3$ and $l = -3$) corresponding to different angular block patterns. It can be observed that as the area of the beams wiretapped by eavesdroppers decreases from 31/32 (1/32-block) to 1/32 (31/32-block), the desired OAM orders and the power difference between adjacent orders gradually decrease. To assess the security of the communication system, we here use the power of the desired channel and the cross talk between the multiplexed channels in the eavesdropped optical field as evaluation metrics. This is because once the eavesdropper's access to the power of the required channel is

reduced, the spontaneous radiation noise introduced by the optical amplifier in the receiving system will lower the OSNR of the signal, thus decreasing the accuracy of the eavesdropper in obtaining the original information. On the other hand, an increase in the cross talk between the multiplexed channels will enhance the interference experienced by the eavesdropper when he is trying to obtain other signals within the required channel. This can severely affect the accuracy of the eavesdropper in obtaining the original information. Therefore, in a communication system, if the power of the required channel in the portion of the optical field energy obtained by the eavesdropper is low and the cross talk between the multiplexed channels is high, this indicates that the communication system has a higher level of security. Conversely, it is considered insecure. We then simulate the normalized power of the required OAM beam with $l = +3$ and the cross talk between OAM beams with $l = +3$ and $l = -3$ when the eavesdropper wiretaps on different beam sizes, as shown in Fig. 5(c3). One can indicate that as the area of the beams wiretapped by eavesdroppers decreases from 63/64 (1/64-block) to 1/64 (63/64-block), the normalized power of the desired OAM beam with $l = +3$ decreases from -0.19 to -35.92 dB. At the same time, the cross talk between OAM beams with $l = +3$ and $l = -3$ increases from -35.84 to -0.11 dB. To further evaluate the security of the communication system, we analyze the eavesdropper in a general scenario, as shown in Figs. 5(d1)–5(d3). In this scenario, we assume that the eavesdropper has a finite circular aperture and wiretaps at different positions across the beam cross section. Figures 5(d1) and 5(d2), respectively, show the OAM order spectra obtained by eavesdroppers for individual OAM beams ($l = +3$) and two OAM multiplexed beams ($l = +3$ and $l = -3$) at different aperture offsets, where the aperture radius of eavesdropper r_e is equal to that of an OAM beam with $l = +3$ r_b . It can be seen that as the eavesdropper's aperture offset increases from $0.5r_b$ to $2r_b$, the power of the required OAM beam with $l = +3$ and $l = -3$ rapidly decreases, and the power difference between adjacent channels sharply decreases. Figure 5(d3) shows the simulated normalized power of an OAM beam with $l = +3$ and cross talk between OAM beams with $l = +3$ and $l = -3$ as functions of the eavesdropper's aperture offset. It can be observed that as the eavesdropper's aperture radius decreases from $1.5r_b$ to $0.5r_b$, the eavesdropper's aperture offset increases from 0 to $2r_b$, the power of the OAM beam of the required channel rapidly decreases, and the cross talk values between two multiplexed channels increase sharply. From the results above, we can see that whether the eavesdropper is co-axial with the OAM beam or situated in a general off-axis scenario, once the eavesdropper only obtains a small part of the light field distribution, the power of the required channel and the cross talk values between different multiplexed channels make it difficult for the eavesdropper to recover the original information, thus confirming the high security of the communication system.

In practical optical communications, it is challenging for eavesdroppers to obtain most of the optical fields demonstrated in the experiment. This is because wiretapping too much optical field energy would result in significantly reduced energy at the receiver's end of the original communication system, leading to a deterioration in communication quality and raising the receiver's awareness. Furthermore, it is difficult for eavesdroppers to guarantee that the wiretapped optical field has the ideal angular distribution characteristics demonstrated in the experiment,

which increases the difficulty of demodulating OAM modes and the cross talk between different channels. Considering that eavesdroppers also need to account for the trial-and-error difficulty of attempting different mode numbers when demodulating OAM modes, it becomes challenging for eavesdroppers to obtain the desired information in an FSO communication system based on OAM mode multiplexing. Therefore, the experiment results validate the possibility of eavesdroppers obtaining communication link information in an extreme ideal scenario, confirming the high security of the FSO communication system based on OAM mode multiplexing.

2.4 260-m Power-Controllable 1-to-9 Multicasting Interconnects Link

When it comes to the situation of one-to-many or many-to-many data distribution in some remote areas, war zones, and temporary stations, hundreds of meters of multicasting in FSO interconnects is always the best option. Here we also demonstrate a 260-m power-controllable 1-to-9 multicasting interconnect link.

Considering different influences for different OAM orders resulting from atmospheric turbulence and other reasons, such as slight displacement at the receiver side, the power loss of different topological charges is quite different, and the relationship is nonlinear. In fact, we ignore the exact relationship among the OAM orders and various possible reasons but just care about the output power and input power like a black box. So we establish an offline feedback process between the output and input and change the complex power-controllable multicasting pattern^{42,43} on the transmitter side continually to achieve the desired power target (refer to Fig. S4 in the [Supplementary Material](#)). When we transmit 1-to-9 multicasting at the same power designed on the pattern, the nine channels ($l = 0, \pm 1, \pm 2, \pm 3, \pm 4$) produce different power losses resulting from real-time atmospheric turbulence and other reasons, as shown in Fig. 6(a1). The power distinction between the largest multicasting channel and the least one is about 9 dB, while it is about 6 dB between the least power multicasting channel and the undesired channel. For examining the power-controllable offline feedback process, we demonstrate how to correct each channel to achieve nearly the same power distribution. In Fig. 6(a2), the interchannel power distinction reduces to about 2.4 dB, and it remains about 6 dB between the least power multicasting channel and the undesired channel. The intensity profiles of 1-to-9 OAM multicasting before and after such offline feedback process are presented in Fig. S5 in the [Supplementary Material](#). In many practical scenarios, the different users (different channels) may require different powers according to the distance or other reasons. The power-controllable offline feedback process we demonstrated can not only correct the power distribution affected by atmospheric turbulence but also provide flexible control of the power distribution in practical applications. We also investigate the BER performance [Fig. 6(b)] for power-controllable 1-to-9 multicasting interconnects link as the power distribution shown in Fig. 6(a2). All the nine BER curves (including Gaussian) almost huddle together, and the average OSNR penalty is about 2 dB at the EFEC limit of 2×10^{-3} .

For OAM beam multicasting interconnects, we also need to analyze their security. In OAM beam multicasting systems, since each multicasting channel carries the same information, there is no cross-talk-induced interference between different

multicasting channels. The eavesdropper only needs to detect the multicasting channels carrying the information. In this case, we use the average power of the multicasting channels obtained by the eavesdropper as the evaluation metric. The lower the average power of the multicasting channels obtained by the eavesdropper, the more susceptible the signal is to noise interference, making it easier to reduce the accuracy of the eavesdropper's retrieval of the original information, indicating higher security for the multicasting interconnect system. Figure 6(c1) depicts the simulated OAM order spectra obtained by eavesdroppers for nine multicasting channels ($l = 0, \pm 1, \pm 2, \pm 3, \pm 4$) corresponding to different angular block patterns. It can be seen that as the area of the beams wiretapped by eavesdroppers decreases from 31/32 (1/32-block) to 1/32 (31/32-block), the power of the desired multicasting channels gradually decreases. We then simulate the average power of the multicasting channels when the eavesdropper wiretaps on different beam sizes, as shown in Fig. 6(c2). One can indicate that as the area of the beams wiretapped by eavesdroppers decreases from 63/64 (1/64-block) to 1/64 (63/64-block), the average power of the multicasting channels decreases from -14.66 to -38.44 dB. We then evaluate the security of the multicasting interconnect system in a general scenario as shown in Figs. 6(d1) and 6(d2), where the aperture radius of eavesdropper r_e is equal to that of the OAM beam with $l = +4 r_b$. Figure 6(d1) shows the OAM order spectra obtained by eavesdroppers for nine multicasting channels at different aperture offsets. Figure 6(d2) displays the simulated average power of nine multicasting channels as functions of the eavesdropper's aperture offset. One can indicate that as the eavesdropper's aperture radius decreases from $1.5r_b$ to $0.5r_b$, and the eavesdropper's aperture offset increases from 0 to $2r_b$, the average power of nine multicasting channels rapidly decreases. This result indicates that once the eavesdropper obtains only a portion of the optical field distribution, the average power of nine multicasting channels acquired by the eavesdropper decreases, making it difficult for the eavesdropper to accurately recover the original information, validating the security of the multicasting system.

3 Conclusion and Discussion

We demonstrate a 260-m secure optical interconnect link employing 10-Gbaud (40-Gbit/s) 16-QAM carrying OAM multiplexing; a power-controllable 1-to-9 multicasting link is also investigated. First, we study the beam wandering, received power fluctuation, and channel cross talk after 260-m propagation. It is obvious that the beam displacement and power fluctuation after beam reduction remains stable even with 260-m atmospheric turbulence. For multiplexing, the average interchannel cross talk is less than -20 dB for $l = +3$ and $l = -3$. Meanwhile, for multicasting, the average cross talk for the desired channel and the undesired channel is less than -6 dB. Furthermore, we study the BER performance and link security. The results show that our 260-m optical interconnect link works well for both security OAM multiplexing and power-controllable 1-to-9 multicasting. The eavesdropper cannot recover the correct data information when he wiretaps just a part of OAM beams. The more OAM beams are blocked, the more errors are received by the eavesdropper. Only complete reception of OAM beams corresponds to the best BER performance. As for multicasting application, an offline feedback process works for improving the link property and also maintaining flexible control of the power distribution for practical applications.

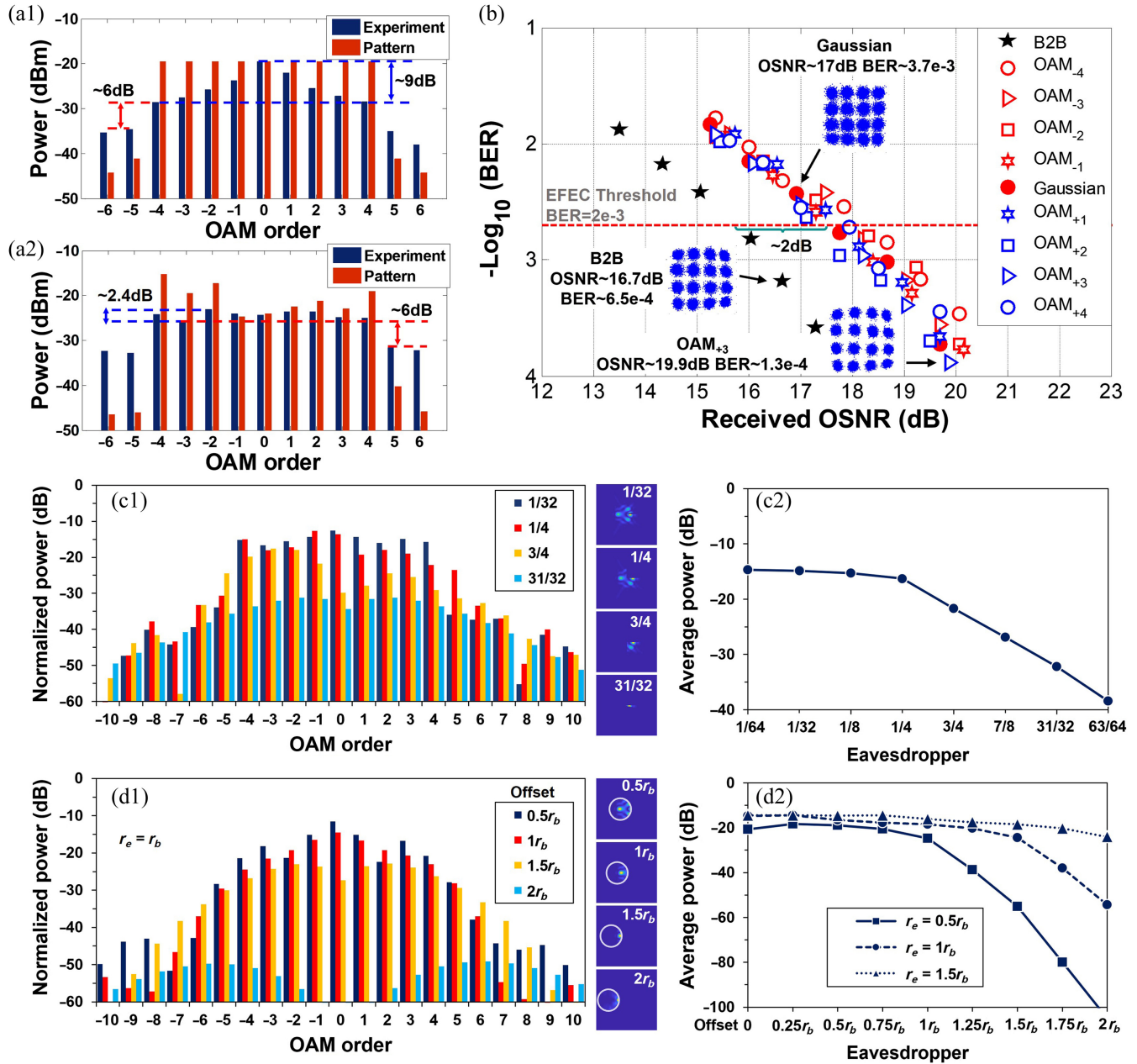


Fig. 6 BER performance for multicasting. (a1), (a2) Multicasting power of pattern-designed and experiment before and after offline feedback process respectively. (b) Measured BER performance for 260-m power-controllable 1-to-9 multicasting interconnects link. (c1) Simulated OAM order spectra of multicasting OAM beams wiretapped by the eavesdropper with angular block. Insets are intensity profiles wiretapped by the eavesdropper. (c2) Simulated average power of multicasting channels wiretapped by the eavesdropper with angular block. (d1) Simulated OAM order spectra of multicasting OAM beams wiretapped by the eavesdropper in a general scenario. Insets are intensity profiles wiretapped by the eavesdropper. r_e : eavesdropper's aperture radius. r_b : OAM beam radius of $l = +4$ transmitted over 260 m. (d2) Simulated average power of multicasting channels wiretapped by the eavesdropper in a general scenario.

For some practical applications, such as interbuilding interconnects, such a few hundred FSO link plays an important role and has attracted more and more interest. What is more, by introducing OAM as an orthogonal SDM modal basis set, the system capacity and spectral efficiency have dramatically increased, which will provide an alternative option for solving

the capacity crunch brought by the booming of optical interconnects. Security is another advantage of employing OAM multiplexing; it is hard to wiretap information from an invisible channel in free space. Additionally, multicasting is a critical technique for some one-to-many or many-to-many applications. Considering the distinguishing power loss between different

multicasting channels, it is necessary to introduce a feedback process to correct or even control the power distribution. The power-controllable multicasting phase pattern we designed can not only flexibly control the power distribution but also simultaneously generate multiple OAM modes in a single phase-only SLM. Although the offline feedback process we adopted does not change in real time because of atmospheric turbulence, for weak turbulence it can still handle the problem with good consequences.

4 Appendix: Supplementary Information

The [Supplementary Material](#) containing Secs. S1–S8 and Figs. S1–S8 is available at <https://doi.org/10.1117/1.APN.3.1.016004.s01>. In addition to the [Supplementary Material](#), the following supplementary video is included:

Video 1. Beam displacement after beam reduction of $l = -3$, MP4, 4.65 MB [URL: <https://doi.org/10.1117/1.APN.3.1.016004.s1>].

Disclosures

The authors declare that there are no conflicts of interest regarding the publication of this article.

Code and Data Availability

Data underlying the results presented in this paper are not publicly available at this time but may be obtained from the authors upon reasonable request.

Acknowledgments

This work was supported by the National Natural Science Foundation of China (Grant Nos. 62125503, 62261160388, and 62101198), the Natural Science Foundation of Hubei Province of China (Grant Nos. 2021CFB011 and 2023AFA028), the Key R&D Program of Hubei Province of China (Grant Nos. 2020BAB001 and 2021BAA024), Shenzhen Science and Technology Program (Grant No. JCYJ20200109114018750), and the Innovation Project of Optics Valley Laboratory (Grant Nos. OVL2021BG004 and OVL2023ZD004). The authors thank Yongxiong Ren at University of Southern California for helpful discussions.

References

- R. W. Tkach, "Scaling optical communications for the next decade and beyond," *Bell Labs Tech. J.* **14**, 3–9 (2010).
- E. Ciaramella, et al., "1.28-Tb/s (32×40 Gb/s) free-space optical WDM transmission system," *IEEE Photonics Technol. Lett.* **21**, 1121–1123 (2009).
- A. Turpin et al., "Free-space optical polarization demultiplexing and multiplexing by means of conical refraction," *Opt. Lett.* **37**, 4197–4199 (2012).
- P. J. Winzer, "Modulation and multiplexing in optical communication systems," in *IEEE LEOS Newslett.*, **23**, 4–10 (2009).
- G. Gibson, J. Courtial, and M. J. Padgett, "Free-space information transfer using light beams carrying orbital angular momentum," *Opt. Express* **12**, 5448–5456 (2004).
- J. Wang et al., "Terabit free-space data transmission employing orbital angular momentum multiplexing," *Nat. Photonics* **6**, 488–496 (2012).
- L. Allen et al., "Orbital angular momentum of light and the transformation of Laguerre–Gaussian laser modes," *Phys. Rev. A* **45**, 8185–8189 (1992).
- S. Franke-Arnold, L. Allen, and M. Padgett, "Advances in optical angular momentum," *Laser Photonics Rev.* **3**, 299–313 (2008).
- A. M. Yao and M. J. Padgett, "Orbital angular momentum: origins, behavior, and applications," *Adv. Opt. Photonics* **3**, 161–204 (2011).
- K. Dholakia and T. Čížmár, "Shaping the future of manipulation," *Nat. Photonics* **5**, 335–342 (2011).
- L. Paterson et al., "Controlled rotation of optically trapped microscopic particles," *Science* **292**, 912–914 (2001).
- M. P. MacDonald et al., "Creation and manipulation of three-dimensional optically trapped structures," *Science* **296**, 1101–1103 (2002).
- M. Padgett and R. Bowman, "Tweezers with a twist," *Nat. Photonics* **5**, 343–348 (2011).
- K. Toyoda et al., "Using optical vortex to control the twisted metal nanostructures," *Nano Lett.* **12**, 3645–3649 (2012).
- M. R. Dennis et al., "Isolated optical vortex knots," *Nat. Phys.* **6**, 118–121 (2010).
- S. Bernet et al., "Quantitative imaging of complex samples by spiral phase contrast microscopy," *Opt. Express* **14**, 3792–3805 (2006).
- N. M. Elias, II, "Photon orbital angular momentum in astronomy," *Astron. Astrophys.* **492**, 883–922 (2008).
- A. Mair et al., "Entanglement of the orbital angular momentum states of photons," *Nature* **412**, 313–316 (2001).
- G. Molina-Terriza, J. P. Torres, and L. Torner, "Twisted photons," *Nat. Phys.* **3**, 305–310 (2007).
- J. T. Barreiro, T.-C. Wei, and P. G. Kwiat, "Beating the channel capacity limit for linear photonic superdense coding," *Nat. Phys.* **4**, 282–286 (2008).
- E. Nagali et al., "Optimal quantum cloning of orbital angular momentum photon qubits through Hong–Ou–Mandel coalescence," *Nat. Photonics* **3**, 720–723 (2009).
- J. Leach et al., "Quantum correlations in optical angle-orbital angular momentum variables," *Science* **329**, 662–665 (2010).
- N. Bozinovic et al., "Terabit-scale orbital angular momentum mode division multiplexing in fibers," *Science* **340**, 1545–1548 (2013).
- J. Wang et al., "N-dimensional multiplexing link with 1.036-Pbit/s transmission capacity and 112.6-bit/s/Hz spectral efficiency using OFDM-8QAM signals over 368 WDM Pol-Muxed 26 OAM modes," in *Proc. Eur. Conf. Opt. Commun. (ECOC)*, Cannes, France, p. Mo.4.5.1 (2014).
- J. Wang et al., "Ultra-high 435-bit/s/Hz spectral efficiency using N-dimensional multiplexing and modulation link with pol-muxed 52 orbital angular momentum (OAM) modes carrying Nyquist 32-QAM signals," in *Proc. Eur. Conf. Opt. Commun. (ECOC)*, Valencia, Spain, p. Th.2.5.4 (2015).
- D. L. Begley, "Free-space laser communications: a historical perspective," in *Proc. Annu. Meet. IEEE LEOS*, Glasgow, UK, Vol. **3**, pp. 391–392 (2002).
- W. S. Rabinovich et al., "Free space optical communications research at the US Naval Research Laboratory," *Proc. SPIE* **7587**, 758702 (2010).
- A. H. Hashim et al., "Modeling and performance study of inter-satellite optical wireless communication system," in *Proc. Int. Conf. Photonics*, IEEE (2010).
- D. Divsalar and F. Pollara, "Multiple turbo codes for deep-space communications," The Telecommunications and Data Acquisition Report, 66–77 (1995).
- K. S. Andrews et al., "The development of turbo and LDPC codes for deep-space applications," *Proc. IEEE* **95**, 2142–2156 (2007).
- T. Komine and M. Nakagawa, "Fundamental analysis for visible-light communication system using LED lights," *IEEE Trans. Consum. Electron.* **50**, 100–107 (2004).
- G. A. Shaw et al., "Recent progress in short-range ultraviolet communication," *Proc. SPIE* **5796**, 214–225 (2005).
- M. Krenn et al., "Communication with spatially modulated light through turbulent air across Vienna," *New J. Phys.* **16**, 113028 (2015).

34. G. Vallone et al., "Free-space quantum key distribution by rotation-invariant twisted photons," *Phys. Rev. Lett.* **113**, 060503 (2014).
35. Y. Ren et al., "Experimental characterization of a 400 Gbit/s orbital angular momentum multiplexed free space optical link over 120 m," *Opt. Lett.* **41**, 622–625 (2015).
36. Y. Zhao et al., "Experimental demonstration of 260-meter security free-space optical data transmission using 16-QAM carrying orbital angular momentum (OAM) beams multiplexing," in *Proc. Opt. Fiber Commun. Conf. (OFC)*, Anaheim, USA, p. Th1H.3 (2016).
37. M. A. Khalighi and M. Uysal, "Survey on free space optical communication: a communication theory perspective," *IEEE Commun. Surv. Tut.* **16**, 2231–2258 (2014).
38. V. W. S. Chan, "Free-space optical communications," *J. Lightwave Technol.* **24**, 4750–4762 (2006).
39. H. A. Willebrand and B. S. Ghuman, "Fiber optics without fiber," *IEEE Spectr.* **40**, 41–45 (2001).
40. E. Leitgeb, "Current optical technologies for wireless access," in *Proc. Int. ConTEL*, Zagreb, Croatia, pp. 7–17 (2009).
41. D. Kedar and S. Arnon, "Urban optical wireless communication networks: the main challenges and possible solutions," *IEEE Commun. Mag.* **42**, S2–S7 (2004).
42. L. Zhu and J. Wang, "Simultaneous generation of multiple orbital angular momentum (OAM) modes using a single phase-only element," *Opt. Express* **23**, 26233 (2015)
43. S. Li and J. Wang, "Adaptive power-controllable orbital angular momentum (OAM) multicasting," *Sci. Rep.* **5** 9677 (2016).
44. L. Li et al., "Performance enhancement of an orbital-angular-momentum-based free-space optical communication link through beam divergence controlling," in *Proc. Opt. Fiber Commun. Conf. (OFC)*, Los Angeles, USA, p. M2F.6 (2015).

Biographies of the authors are not available.